Microchimica Acta (2019) 186: 318
https://doi.org/10.1007/s00604-019-3454-1

SHORT COMMUNICATION

Metal-ion-induced DNAzyme on magnetic beads for detection of lead(II) by using rolling circle amplification, glucose oxidase, and readout of pH changes

Dianping Tang[1] · Biyun Xia[1] · Ying Tang[1] · Jin Zhang[1] · Qian Zhou[2]

Received: 2 March 2019 / Accepted: 15 April 2019 / Published online: 2 May 2019

Abstract

This work reports on a method for determination of lead(II) ion in environmental water samples. A Pb^{2+}-specific DNAzyme immobilized on magnetic beads was coupled to rolling circle amplification (RCA) and pH meter-based readout. On addition of Pb^{2+} ion, it induces partial cleavage of the DNAzyme on the magnetic beads. The single-stranded DNA remaining on the magnetic beads is used as the primer to trigger the RCA reaction with the assistance of a circular DNA template, polymerase and dNTPs. This results in the formation of numerous oligonucleotide repeats on the magnetic bead. Subsequently, these repeats hybridize with glucose oxidase-labeled single-stranded DNA (GOx-ssDNA) to form a long concatamer containing tens to hundreds of GOx-ssDNA tandem repeats. The concatenated GOx molecules oxidize glucose, and this is accompanied by a drop in the local pH value. The pH values (vs. background signal) drop linearly when Pb^{2+} concentrations increase from 1.0–100 nM, and the detection limit is 0.91 nM. The method displays good reproducibility, high specificity and acceptable accuracy. It was applied to the analysis of spiked water samples, and results compared favorably with those obtained by ICP-MS.

Keywords Environmental water samples · Magnetic Fe_3O_4 nanoparticles · ICP-MS · Glucose oxidase-labeled single-strand DNA · Target-induced rolling cycle amplification

Introduction

Magnetic beads have been demonstrated intensively as an ideal protein host since they have highly chemical stability and relatively environmental inertness [1, 2]. Nanometer-sized Fe_3O_4 particles have high-surface hydroxyl groups which are favorable for a wide variety of surface reactions and the binding of biomolecules including proteins, DNA and peptides [3, 4]. The bionanocomposites are readily separated from the mixtures with an aid of external magnetic field [5]. Thanks to these advantages, research has looked to explore innovative and powerful novel biofunctionalized nanometer-sized magnetic beads, controlling and tailoring their properties in a very predictable manner to meet the needs of specific applications because of high surface-to-volume ratio relative to bulk materials [6, 7].

Magneto-controlled biosensors and bioelectronics examine the effects of external magnetic fields on the electrical signals

Dianping Tang and Biyun Xia contributed equally to this work.

Electronic supplementary material The online version of this article (https://doi.org/10.1007/s00604-019-3454-1) contains supplementary material, which is available to authorized users.

✉ Dianping Tang
dianping.tang@fzu.edu.cn

✉ Qian Zhou
zhouqian@henu.edu.cn

[1] Chongqing Key Laboratory of Environmental Materials & Remediation Technologies, Chongqing University of Arts and Sciences, Chongqing 402160, People's Republic of China

[2] Institute of Environmental and Analytical Science, School of Chemistry and Chemical Engineering, Henan University, Kaifeng 475004, People's Republic of China

(e.g., current, voltage, resistance or capacitance) of functionalized magnetic beads associated with the electrodes [8]. Typically, there are two basic concerns on the successful development of high-efficiency magnetic biosensing systems. Undoubtedly, the first key point relies on the signal-transduction method and device. A pH meter, a device used for potentiometric pH measurements toward the hydrogen-ion activity in water-based solutions, works by measuring the potential difference with a pH (proton)-sensitive electrode (usually glass) and a reference electrode (usually silver chloride or calomel) [9]. Ideally, the electrode potential, E (mV), for the proton depends on the logarithm of hydronium ion in the activity followed by the Nernst equation [10]. Digital or handheld pH meters have been developed for the bioanalytical applications because of its simple operation, portability and easy quantification [11, 12]. Liang et al. designed pH meter-based electrochemical immunoassay for the detection of neuron-specific enolase using glucose oxidase-loaded liposome [13]. Wang et al. developed portable, self-powered, and light-addressable photoelectrochemical sensing platforms using pH meter readouts for high-throughput screening of thrombin inhibitor drugs [14]. Jakhar and Pundir prepared urease nanoparticles for the construction of an improved potentiometric pH urea biosensor [15]. Thus, our motivation of this study is to design a portable and magneto-controlled pH meter-based detection method for the analytical applications.

Another additional issue for the development of pH meter-based method depends on the signal amplification during the signal-generation process. Enzymes, e.g., glucose oxidase (GOX) and alkaline phosphate, are usually used for this purpose via enzymatic conversion of certain substrates or chemical decomposition of its soluble salts. However, the detectable signal is always limited thanks to the limitation of magnetic beads in surface coverage. Inspiringly, the emergence of DNA-based signal amplification strategies opens a new horizon by coupling with enzyme labels, e.g., hybridization chain reaction and rolling circle amplification (RCA) [16–18]. As a simplified version of natural rolling circle replication, RCA describes a process of unidirectional nucleic acid replication that can rapidly synthesize multiple copies of circular molecules of DNA or RNA [19]. Different from conventional DNA amplification techniques (e.g., polymerase chain reaction), RCA is an isothermal nucleic acid amplification technique where the polymerase continuously adds single nucleotide to a primer annealed to a circular template which results in a long concatamer single-stranded DNA (ssDNA) that contains tens to hundreds of tandem repeats (complementary to the circular template) [20, 21]. In the case, the formed repeats can hybridize with another ssDNA (similar to the circular template). When enzyme molecule is labeled to the ssDNA, the formed repeats hybridize to generate a long enzyme concatamer, thus causing the enzymatic conversion of numerous substrates [22]. Relative to magnetic bead alone, the conjugated enzyme molecules largely increase, thereby resulting in the signal amplification. To this end, RCA is expected to enhance the signal of magneto-controlled pH meter-based assay.

This report designs a sensitive and portable pH meter-based magnetic detection method for lead ion (Pb^{2+}) by coupling with rolling circle amplification on magnetic beads (Scheme 1). This system involves in Pb^{2+}-specific reaction with DNAzyme-coated magnetic bead, primer-triggered RCA reaction, hybridization of glucose oxidase-labeled ssDNA (GOx-ssDNA) and oxidization of GOx toward the substrate (glucose). Upon cleavage of Pb^{2+}-specific DNAzyme, the formed GOx tandem repeats oxidizes glucose into gluconic acid and hydrogen peroxide. The produced gluconic acid changes the pH value of detection solution which is detected on a portable pH meter. The pH shift of

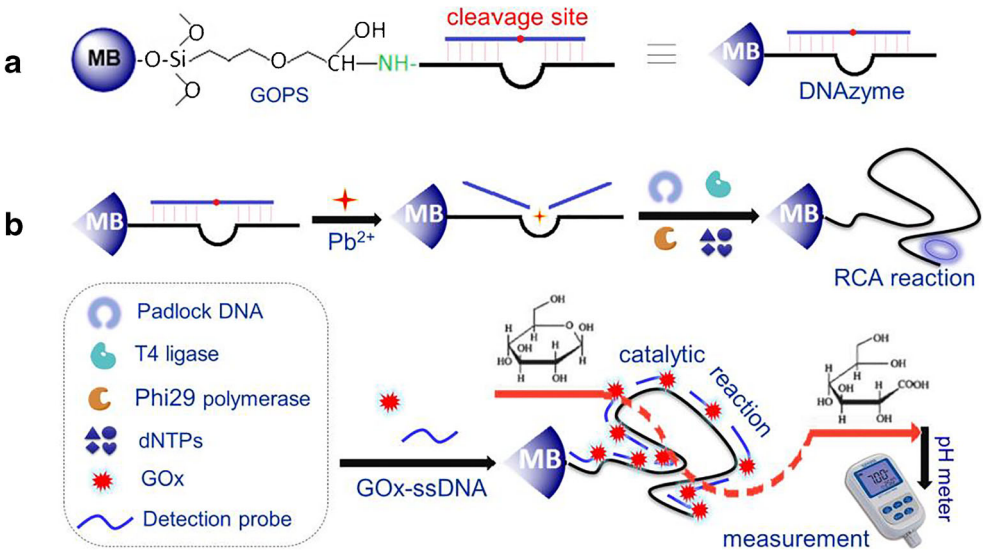

Scheme 1 Schematic illustration of metal-ion-induced DNAzyme on magnetic bead (MB) for the detection of lead ion (Pb^{2+}) with rolling circle amplification (RCA) on a handheld pH meter: **a** preparation process of Pb^{2+}-specific DNAzyme on the magnetic bead, and **b** pH meter-based detection process by coupling with the RCA reaction and hybridization of glucose oxidase-labeled single-stranded DNA probe (GOx-ssDNA)

the detection solution relative to background signal depends on the level of target Pb^{2+} in the sample. This study aims to explore a portable and sensitive magneto-controlled pH meter-based detection system for heavy metal ions in the environmental water samples.

Experimental

Reagent and chemical

Aqueous dispersion of magnetic nanoparticles with hydrodynamic diameter of 100 nm (25 mg mL^{-1}; Number of particles: ~1.8×10^{15}/g; Density: ~5.2 g cm^{-3}; Storage: ddH_2O) was purchased from Chemicell GmbH (Eresburgstrasse 22–23, Berlin, Germany www.chemicell.com). Bovine serum albumin (BSA; Vetec™ reagent grade, lyophilized powder, ≥98%), (3-glycidyloxypropyl) trimethoxysilane (GOPS; ≥98%), glucose oxidase (GOx; Type X-S; lyophilized powder; 100,000–250,000 units g^{-1} solid without added oxygen), D-glucose, sulfosuccinimidyl-4-(*N*-maleinidomethyl)-cyclohexane-1-carboxylat (sulfo-SMCC) and tris(2-carboxyethl) phosphine (TCEP) were gotten from Sigma-Aldrich (www.sigmaaldrich.com). Deoxyribonucleoside 5′-triphosphates mixture (dNTP), T4 DNA ligase (Activity: 5000 units mL^{-1}), adenosine 5′-triphosphate (ATP) and phi29 DNA polymerase (Activity: 10,000 units mL^{-1}) were purchased from Takara Biotechnol. Co., Ltd. (Dalian, China www.takara.com.cn). All other reagents were of analytical grade and used without further purification. Ultrapure water obtained from a Millipore water purification system was used in all runs (18.2 MΩ cm, Milli-Q, Millipore www.millipore.com). All buffers including phosphate-buffered saline (PBS) solutions with various pH values were the products of Sigma-Aldrich (www.sigmaaldrich.com).

All used oligonucleotides were obtained from Sangon Biotech. Co., Ltd. (Shanghai, China www.sangon.com), and their sequences were listed as follows:

Catalytic strand: 5'-NH_2-TTT CAT CTC TTC TCC GAG **CCG GTC GAA ATA GTG AGT**-3'
Substrate strand: 5'-ACT CAC TAT **rA** GGA AGA GAT G-3'
Circular template: 5′-p-*TTC GAC CGG* AAC TGT CTT AGC AAA AAC TGT CTT AGC AA*A CTC ACT AT*-3′
Detection probe: 5'-SH-ACT CAC TAT TTC GAC CGG-3'

Pb^{2+}-specific DNAzyme was designed according to our previous report [23]. The bold sequence at the catalytic strand was the primer for the RCA reaction. The italicized sequence at the circular template ($p = 5'$ phosphate) matched the bold bases of the catalytic strand. The detection DNA probe was the same as those in the italic on the circular template. GOx-labeled single-stranded DNA (i.e., detection probe) was prepared according to this literature [24], and described in the Electronic Supporting Material.

Preparation of Pb^{2+}-specific DNAzyme-conjugated magnetic bead (DNAzyme-MB)

Before synthesis of DNAzyme-MB, the aminated DNA catalytic strands were covalently conjugated onto magnetic beads through the epoxy-amino reaction [25]. In detail, magnetic beads obtained by magnetic separation were initially dried in the vacuum at 80 °C for 60 min. Thereafter, magnetic beads (250 mg) were added to the GOPS dry toluene (5.0 mL, 5%, *v*/v) and stirred for 12 h (500 rpm, RT). Following that, the suspension was magnetically separated, and washed three times with toluene and ethanol solution, respectively. The GOPS-functionalized magnetic beads (GOPS-MBs) were dried and activated in an oven at 80 °C for 60 min under a nitrogen atmosphere. Afterword, the aminated DNA catalytic strands (100 μL, 1.0 mM) was injected into the GOPS-MB suspension at a concentration of 25 mg mL^{-1}. The mixture was slightly stirred for 12 h at 4 °C for conjugation of amino groups on catalytic strands with epoxy group on the GOPS. Catalytic strand-conjugated MBs by magnetic separation were injected to substrate strand (200 μL, 1.0 mM) in ultrapure water, and incubated for 6 h at 37 °C to make the catalytic strand hybridize with the substrate strand for formation of Pb^{2+}-specific DNAzyme. Finally, the magnetically separated DNAzyme-MBs were dispersed in PBS (10 mM, pH 7.4, 0.1 wt% sodium azide), and stored at 4 °C at a final level of 10 mg mL^{-1}. The conjugation process of DNAzyme-MB is schematically illustrated in Scheme S1 of the Electronic Supporting Material.

Target-induced rolling circle amplification (RCA) and pH meter-based measurement

Target-induced RCA reaction on DNAzyme-MB was initially carried out as follows: (i) 50 μL of Pb^{2+} standard or sample was injected into DNAzyme-MB suspension (10 ng mL^{-1}) in a 1.5-mL centrifugal tube, and reacted for 25 min at RT with slight shaking; (ii) 5.0 μL of circular template DNA (100 nM), 5.0 μL of T4 DNA ligase (4.0 U μL^{-1}), 90 μL of phi29 DNA polymerase (2 unit mL^{-1}) reaction buffer (50 mM, pH 7.5 Tris-HCl buffer, 10 mM magnesium acetate, 33 mM potassium acetate, 1.0 mM dithiothreitol, 10 mM dNTPs, and 0.1% Tween 20) and 1.0-mM ATP were added into the resulting magnetic particles, and incubated for 90 min at RT to conduct the padlock ligation reaction and the RCA reaction; (iii) 100 μL of the GOx-ssDNA was added to the centrifugal tube, and reacted for 120 min at RT; (iv) 200 μL of 2.0 mM (excess) glucose in PBS (10 mM, pH 7.4) was injected into the

centrifugal tube and reacted for 10 min at RT; and (v) the pH of the resulting supernatant was determined on a handheld pH meter (0.00–14.00 pH; ± 0.1 pH, 20 °C; ATC® Aolilong Instr. Inc., Hangzhou, China). Note that the resulting suspension after each step was magnetically separated and washed with PBS (10 mM, pH 7.4). The pH value was collected and registered as the signal relative to target Pb^{2+} concentration. The signals in all experiments referred to average responses of reaction with the corresponding standard deviations in triplicate, unless otherwise indicated. All measurements were performed at room temperature (25 ± 1.0 °C).

Result and discussion

Choice of materials

Scheme 1 gives the schematic illustration of target-induced cleavage of Pb^{2+}-specific DNAzyme on magnetic beads for the sensitive detection of metal ion by coupling rolling circle amplification with pH meter-based readout. In this system, magnetic beads are not only used as the affinity supports of the conjugation of Pb^{2+}-specific DNAzyme, but are favorable for rapid separation and purification after each step. Importantly, this methodology pulls the biomolecules bound to magnetic beads from one laminar flow path to another applying a local magnetic field gradient and selectively removes them from the complex system. Aminated Pb^{2+}-specific DNAzyme is conjugated to magnetic beads through the classical epoxy-amino reaction. Accompanying target-induced cleavage of Pb^{2+}-specific DNAzyme on magnetic beads, the newly produced single-stranded DNA is used as the template for the RCA reaction in the presence of dNTP, thus resulting in a long concatamer ssDNA that contains many tandem repeats (complementary to the circular template). The concatamer repeats are utilized for the reaction with GOx-ssDNA conjugates via the principle of complementary base pairing. In this case, numerous GOx molecules are concatenated together by the RCA product, each of which oxidizes glucose into gluconic acid and hydrogen peroxide. Generation of gluconic acid changes the pH of the detection solution. By monitoring the pH change, the concentration of target Pb^{2+} is exactly evaluated in the sample.

Characterization of DNAzyme-MB and RCA reaction with GOx-ssDNA

For development of magneto-controlled detection platform, preparation of DNAzyme-MB is very crucial to induce target-triggered cleavage of DNAzyme. Figure 1a shows typical scanning electron microscope (SEM; Hitachi S4800, Japan www.hitachi.com) image of the DNAzyme-MB, and the average size was 110 nm in diameter (Fig. 1a, top inset). Most nanoparticles had the similar surface topological structures. The surface became rougher after magnetic beads were finally decorated with many concatenated GOx molecules through the RCA reaction (Fig. 1a, bottom inset). Since the conjugated DNAzyme molecules on the magnetic bead were easily carbonized at high applied voltage, they were difficultly observed in SEM images. To demonstrate this issue, dynamic light scattering (DLS; Zetasizer, Nano S90, Malvern, London, UK www.malvern.com) was employed to investigate the mean sizes and surface potentials of magnetic beads before and after modification with different components including GOPS, catalytic strand and RCA product, respectively (note: Substrate strand did not introduce in this case because the short single-stranded DNA did not almost change obviously the size and surface potential) (Fig. 1b). Clearly, the average sizes of magnetic beads gradually increased after modification with GOPS, catalytic strand, RCA product and GOx-ssDNA in sequence. The increasing size after the RCA reaction was relatively biggest than those of other conjugation components (column '*d*' versus columns '*b*-*c*'), which derived from a long concatamer single-stranded DNA that contains many tandem repeats. Thanks to the presence of surface $-O^-$ groups, the unmodified magnetic beads exhibited a negative zeta potential (−12.2 mV, column '*a*'). Upon the epoxy group introduction, partial $-O^-$ groups were covalently conjugated with the GOPS to form epoxy group-functionalized surface, and the zeta potential decreased to −2.1 mV (column '*b*'). After the aminated catalytic strands reacted with the GOPS via the epoxy-amino reaction, however, the corresponding zeta potential increased to −13.1 mV (column '*c*'), which originated from the negatively charged oligonucleotides. Significantly, the zeta potential of the functional magnetic beads because more negative (−33.4 mV, column '*d*') after RCA reaction, indicating formation of long-oligonucleotide strands. Since the isoelectrical point (*I*p) of GOx is ~4.9, it is negatively charged in PBS (10 mM, pH 7.4). Therefore, the zeta potential of magnetic beads MBs after the final decoration with many concatenated GOx molecules was −78.3 mV (column '*e*'). These results preliminarily indicated that the aminated catalytic strands were conjugated to magnetic beads.

Logically, one puzzling question arises as to whether Pb^{2+}-specific DNAzyme was modified onto the magnetic beads. To clarify this concern, UV-vis absorption spectroscopy was used to monitor magnetic beads before and after formation of DNAzyme-MB (Fig. 1c). Curve '*a*' represents UV-vis absorption spectrum of the unmodified magnetic beads, and almost no characteristic peaks were observed. Also, GOPS-modified magnetic beads gave the similar UV-vis absorption spectrum with magnetic beads alone (curve '*b*'). Favorably, an obvious characteristic absorption peak for the oligonucleotides was acquired at 260 nm (curve '*c*'), suggesting that the aminated catalytic strands were conjugated to magnetic beads. To further verify that Pb^{2+}-specific DNAzyme was formed by the

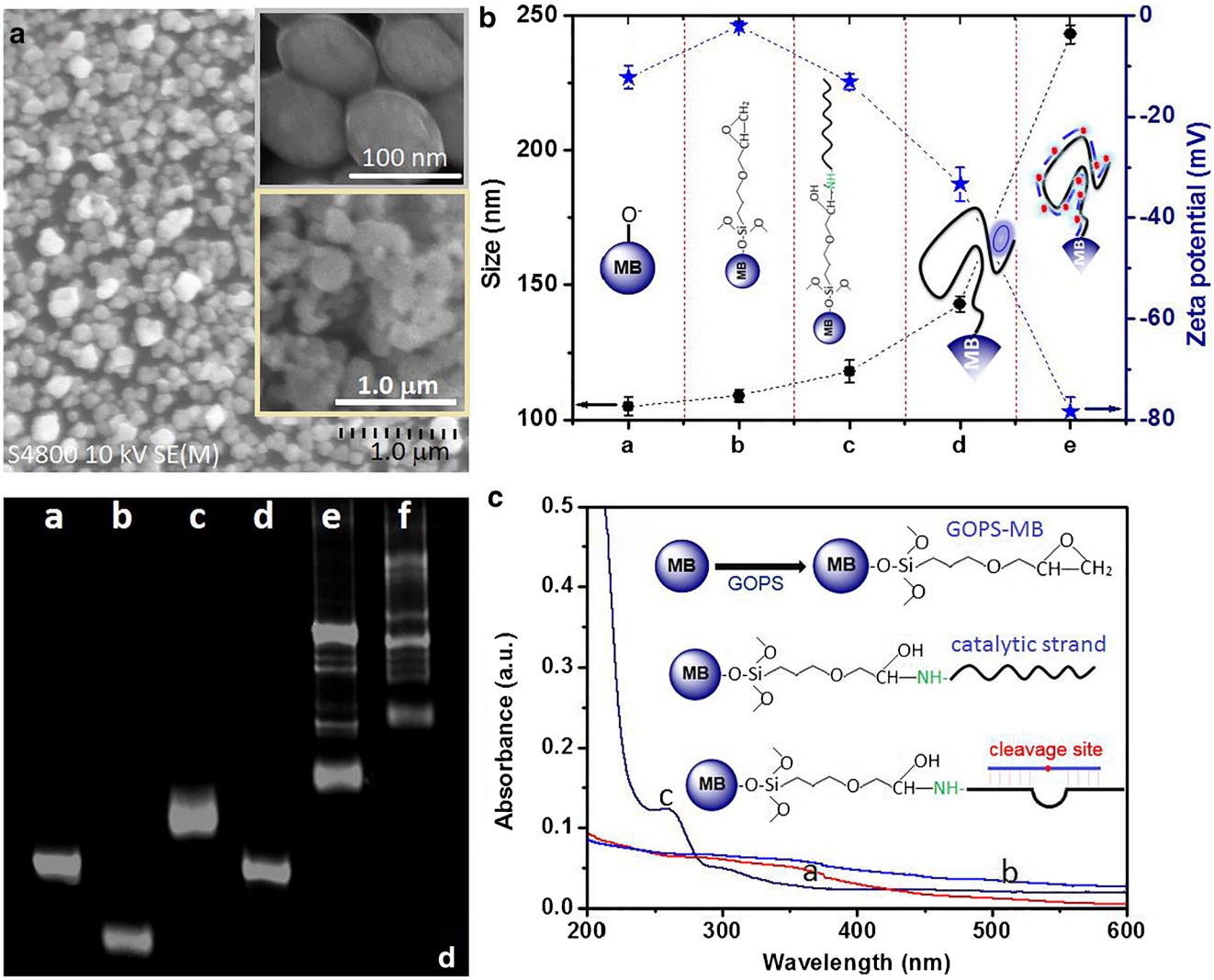

Fig. 1 **a** SEM image of DNAzyme-MB (top inset: magnification image of DNAzyme-MB; bottom inset: SEM image of MBs after the final decoration with many concatenated GOx molecules); **b** DLS data and zeta potentials of ***a*** magnetic bead, ***b*** GOPS-MB, ***c*** catalytic strand-conjugated MB, ***d*** catalytic strand-conjugated MB after RCA reaction and ***e*** MBs after the final decoration with many concatenated GOx molecules; **C** UV-vis absorption spectra of ***a*** magnetic beads, ***b*** GOPS-MB and ***c*** catalytic strand-conjugated MB; and **D** agarose gel electrophoresis images for ***a*** 1.0-μM catalytic strand, ***b*** 1.0-μM substrate strand, ***c*** 1.0-μM catalytic strand +1.0-μM substrate strand, ***d*** DNAzyme +100-nM Pb^{2+}, ***e*** DNAzyme +100-nM Pb^{2+} + RCA reaction and ***f*** DNAzyme +100-nM Pb^{2+} + RCA reaction + GOx-ssDNA

catalytic strand, gel electrophoresis was also utilized to characterize these processes including target-triggered HCR reaction (note: Because the big-sized magnetic beads were not migrated in gel electrophoresis, these experiments were carried out in the absence of magnetic beads) (Fig. 1d). Lanes '*a*' and '*b*' represent the gel electrophoresis images of catalytic strands and substrate strands, respectively. As seen from lane '*c*', the DNA duplex was formed after mixture of catalytic strands with substrate strands. Inspiringly, the formed DNA duplex was cleaved in the presence of target Pb^{2+} (lane '*d*'), because the base number of the spot was almost the same as lane '*a*', indicating the formation of Pb^{2+}-specific DNAzyme. Lane '*e*' shows the products of the cleaved DNAzyme by Pb^{2+} after the RCA reaction. Actually, the fuzzy spot lanes stemmed from the RCA products with different lengths of oligonucleotide strands. Note that the similar results were obtained when RCA products reacted with GOx-ssDNA (lane '*f*'). These results adequately revealed that target-induced DNAzyme on magnetic beads with the RCA reaction was used for the detection of Pb^{2+} through the GOx-ssDNA.

Control tests and analysis of feasibility

As mentioned above, the signal readout derived from the backfilling GOx-ssDNA after the RCA reaction. As control tests, two crucial points should be investigated prior to experiments: (i) whether target-induced RCA reaction was readily progressed step by step, and (ii) whether GOx-ssDNA was nonspecifically conjugated to DNAzyme-MB. Figure 2a displays the pH responses of this system after each step in the

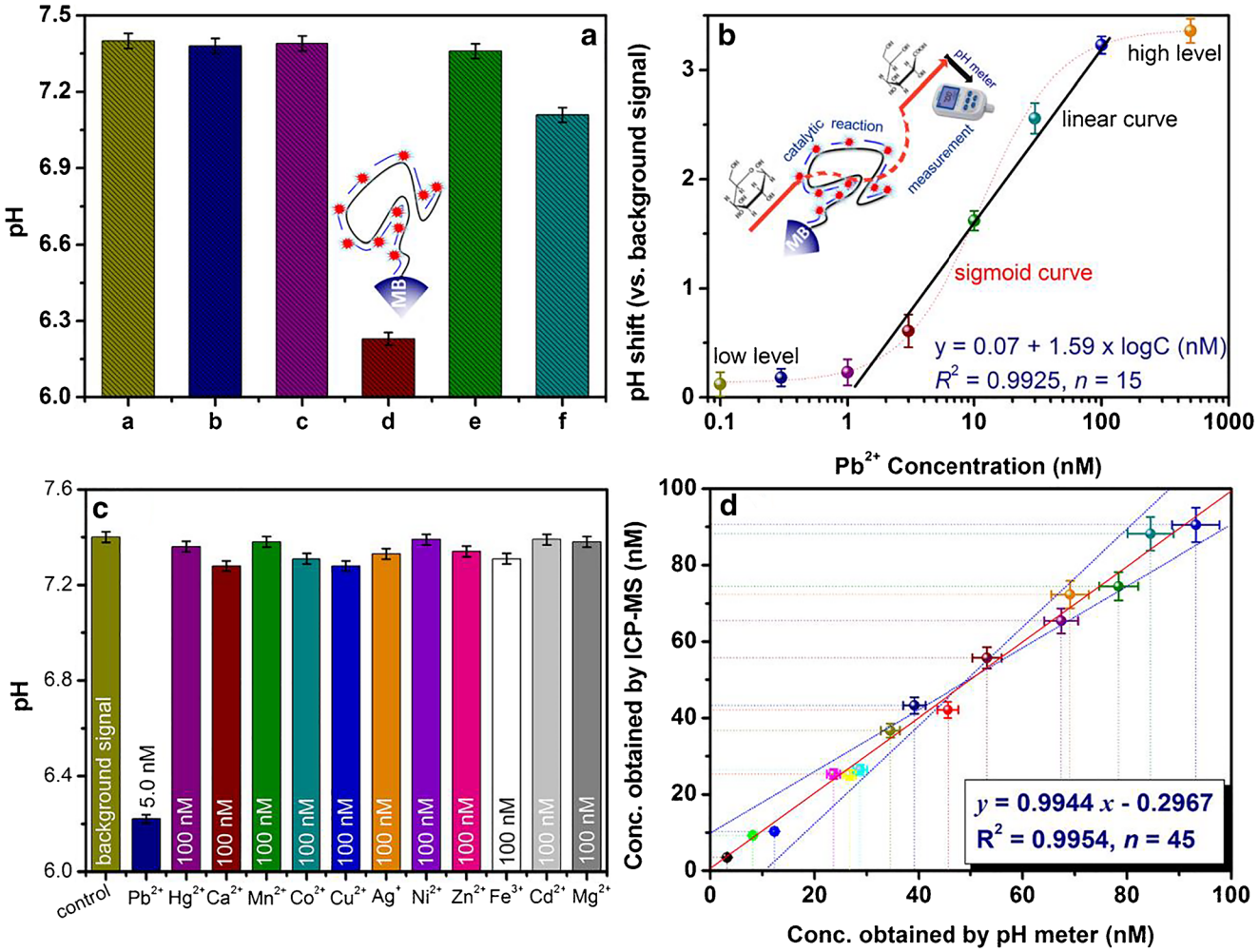

Fig. 2 **a** The pH responses of different components in the presence of glucose (200 μL, 2.0 mM) in PBS (10 mM, pH 7.4): ***a*** DNAzyme-MB, ***b*** DNAzyme-MB + 5.0 nM Pb^{2+}, ***c*** DNAzyme-MB + 5.0 nM Pb^{2+} + RCA reaction, ***d*** DNAzyme-MB + 5.0 nM Pb^{2+} + RCA reaction + GOx-ssDNA, ***e*** DNAzyme-MB + RCA reaction + GOx-ssDNA and ***f*** DNAzyme-MB + 5.0 nM Pb^{2+} + GOx-ssDNA; **b** pH responses (versus background signal) of RCA-based detection platform toward different-concentration Pb^{2+} standards; **C** the specificity of RCA-based Pb^{2+} detection platform; and D comparison of the results obtained from RCA-based Pb^{2+} detection method and ICP-MS for spiked water samples

presence of glucose (200 μL, 2.0 mM) in PBS (10 mM, pH 7.4). Expectedly, almost no pH changes (versus background signal) were observed when DNAzyme-MB (column '*b*') reacted with 5.0 nM Pb^{2+} (column '*c*') and RCA reaction (column '*d*') in turn, indicating that the conjugated DNAzyme and RCA products on magnetic beads were not change the pH value of the detection solution. When the RCA products formed on magnetic beads incubated with GOx-ssDNA, significantly, the pH value of the detection solution (column '*d*') was obviously lower than that of background signal (column '*a*'), suggesting that the pH readout originated from the introduction of GOx-ssDNA. Naturally, one question to be produced was whether the pH change stemmed from the nonspecific adsorption of GOx-ssDNA in the absence of target analyte. As indicated from column '*e*', the pH value of the detection solution was almost the same as the background signal. Therefore, the pH change was from target-triggered HCR reaction with GOx-ssDNA. Since the catalytic strand reacted with GOx-ssDNA, the hybridized products were also investigated by using the same assay mode. The pH value of the detection solution (column '*f*') slightly decreased relative to background signal (column '*a*'). Compared with column '*e*', pH response of this system without RCA reaction was largely lower than that with RCA reaction, revealing that RCA reaction amplified the detectable signal of this system. On the basis of these results, a conclusion was made that our strategy had the ability to determine target Pb^{2+} in the sample.

Analytical performance

Before investigating the analytical properties of RCA-based Pb^{2+} assay system with pH meter, the following parameters were optimized: (a) cleavage time for Pb^{2+}-specific DNAzyme on magnetic beads; (b) RCA reaction time of

Table 1 An overview on the reported nanomaterial-based methods for determination of lead ion

Assay method	Materials	Linear range (nM)	LOD (nM)	Ref.
Ultrasonic assisted precipitation	Imprinted polymer	9.7–241	2.8	[26]
Ion-recognizable nanogels	Polyethersulfone membrane	–	1.0	[27]
Electrochemical sensor	Ionic liquid/poly-L-cysteine	4.8–870	0.82	[28]
Electrochemical aptasensor	gold@polypyrrole	0.5–10	0.36	[29]
Impedimetric sensor	GR-5 DNAzyme	1.0–100	0.33	[30]
HPLC	C_{18} silica monolithic column	–	0.36	[31]
Naked eyes	Graphene oxide/AuNP	10–100,000	1.0	[32]
Fluorescence	BSA-Au nanoclusters	10–1000	1.043	[33]
pH meter	Magnetic beads	1.0–100	0.91	This work

primer; (c) hybridization time of RCA products for GOx-ssDNA; Respective data and figures are given in the Electronic Supporting Material (Fig. S1). The following experimental conditions were found to give best results: (a) cleavage time: 25 min; (b) RCA reaction time: 90 min; (c) hybridization time: 120 min. Under optimum conditions, the analytical performance of RCA-based pH assay platform was studied toward Pb^{2+} standards with different concentrations by coupling with rolling circle amplification and pH meter-based readout device. Figure 2b shows the pH changes of this system (relative to background signal) in the presence of target analyte. The signal increased with the increasing Pb^{2+} level, and a good linear relationship between the pH shift and the decimal logarithm of Pb^{2+} concentration was acquired within the dynamic range of 1.0–100 nM. The limit of detection (LOD) was evaluated to 0.91 nM on the basis of $3S/K$ (where K and S stand for the slope of the calibration plot and the standard deviation of blank solution, respectively). The regression equation was $y = 0.07 + 1.59 \times \log C$ (nM, R^2 = 0.9925, $n = 15$). Each data point represented the average value obtained from three different measurements. The maximum relative standard deviation (RSD) was 10.9%, suggesting a good reproducibility of this system. To further elucidate the signal-amplified advantage of our strategy by using RCA reaction, the analytical properties of this system including the linear range and LOD were compared with other detection schemes. As analyzed from Table 1, the LOD of our designed protocol were comparable with other analytical methods, although the linear range was relatively narrow. The reason might be ascribed to the limitation of the labeled amount of magnetic beads toward Pb^{2+}-specific DNAzyme molecules.

Next, the specificity of our designed strategy was evaluated by challenging it against other metal ions including Hg^{2+}, Ca^{2+}, Mn^{2+}, Co^{2+}, Cu^{2+}, Ag^{+}, Ni^{2+}, Zn^{2+}, Fe^{3+}, Cd^{2+} and Mg^{2+}. Significantly, these non-targets did not almost cause the significant pH change of the detection solution (Fig. 2c). An obvious pH shift relative to background signal was achieved toward target Pb^{2+} ion. These results clearly revealed the high specificity of RCA-based Pb^{2+} sensing system. Further, the storage stability of DNAzyme-MB and GOx-ssDNA was measured during a six-month storage period. They were stored at 4 °C when not in use. By using 5.0 nM Pb^{2+} as an example, the pH signals preserved >90% of the initial signal after storage them for 5 months, suggesting a good stability.

Monitoring of environmental water samples

To further monitor the trueness and applicability of RCA-based Pb^{2+} detection system for testing environmental water samples, Pb^{2+} standards with various concentrations were initially spiked into drinking water. Following that, these water samples were determined by using our method and inductively coupled plasma mass spectrometry (ICP-MS; used as a reference method), respectively. The results obtained from two methods are summarized in Fig. 2d. Comparison of the experimental results obtained with RCA-based Pb^{2+} detection system with those of ICP-MS was performed via the use of a least-squares regression method. The regression line was fitted to $y = (0.9944 \pm 0.0266)\ x - (0.2967 \pm 1.3961)$ ($R^2 = 0.9954$, $n = 45$), where x stands for Pb^{2+} concentrations estimated with RCA-based Pb^{2+} detection system and y stands for those of the ICP-MS. The correlation between two methods was investigated by using t-test for comparison of experimental values of the intercept and slope to the ideal situation of zero intercept and slope of 1. As shown in Fig. 2d, the slope and intercept were close to the ideal values '1' and '0', respectively, thus revealing a good agreement between both analytical methods for the analysis of real water samples.

Conclusions

This contribution describes a portable potentiometric Pb^{2+} detection platform using rolling circle amplification on a

handheld pH meter. The Pb^{2+} nanoprobes were prepared on the basis of Pb^{2+}-specific DNAzyme conjugated onto the magnetic beads. Introduction of molecular biological technique (RCA reaction) and enzyme labels were utilized to amplify the detectable signal of this system. Nevertheless, one disadvantage of this method lies in the long reaction time owing to Pb^{2+}-specific cleavage of DNAzyme and DNA-based RCA/hybridization reaction. Therefore, future work should be focusing on improvement of the whole assay time, e.g., by controlling the reaction temperature of DNA reaction.

Acknowledgements Authors acknowledged financial support from the National Natural Science Foundation of China (Grant nos.: 21675029 & 201874022) and the Health-Education Joint Research Project of Fujian Province (Grant no.: WKJ2016-2-15).

Compliance with ethical standards The author(s) declare that they have no competing interests.

References

1. Lin Y, Zhou Q, Zeng Y, Tang D (2018) Liposome-coated mesoporous silica nanoparticles loaded with L-cysteine for photoelectrochemical immunoassay of aflatoxin B_1. Microchim Acta 185:311
2. Gao Z, Xu M, Hou L, Chen G, Tang D (2013) Magnetic bead-based reverse colorimetric immunoassay strategy for sensing biomolecules. Anal Chem 85:6945–6952
3. Mars A, Ben S, Gaied A, Raouafi N (2018) Electrochemical immunoassay for lactalbumin based on the use of ferrocene-modified gold nanoparticles and lysozyme-modified magnetic beads. Microchim Acta 185:449
4. Xu Y, Lu C, Sun Y, Shao Y, Cai Y, Zhang Y, Miao J, Miao P (2018) A colorimetric aptasensor for the antibiotics oxytetracycline and kanamycin based on the use of magnetic beads and gold nanoparticles. Microchim Acta 185:548
5. Yi J, Qin Q, Wang Y, Zhang R, Bi H, Yu S, Liu B, Qiao L (2018) Identification of pathogenic bacteria in human blood using IgG-modified Fe_3O_4 magnetic beads as a sorbent and MALDI-TOF MS for profiling. Microchim Acta 185:542
6. Wu Y, Wang M, Ouyang H, He Y, Zhao X, Fu Z (2018) Teicoplanin-functionalized magnetic beads for detection of *Staphylococcus aureus* via inhibition of the luminol chemiluminescence by intracellular catalase. Microchim Acta 185:391
7. Modh H, Scheper T, Walter J (2018) Aptamer-modified magnetic beads in biosensing. Sensors 18:1041
8. Robertson A, Dahl J, Ougland R, Klungland A (2012) Pull-down of 5-hydroxymethylcytosine DNA using JBP1-coated magnetic beads. Nat Protoc 7:340–350
9. McMahon J, Braca P (1992) An inexpensive parallel interface to a digital pH meter. J Chem Educ 69:a156–a158
10. Kwon D, Joo J, Lee S, Jeon S (2013) Facile and sensitive method for detecting cardiac markers using ubiquitous pH meters. Anal Chem 85:12134–12137
11. Jiang Y, Su Z, Zhang J, Cai M, Wu L (2018) A novel electrochemical immunoassay for carcinoembryonic antigen based on glucose oxidase-encapsulated nanogold hollow spheres with a pH meter readout. Analyst 143:5271–5277
12. Wang L, Chen C, Huang H, Huang D, Luo F, Qiu B, Guo L, Lin Z, Yang H (2018) Sensitive detection of telomerase activity in cancer cells using portable pH meters as readout. Biosens Bioelectron 121: 153–158
13. Liang J, Wang J, Zhang L, Wang S, Yao C, Zhang Z (2019) Glucose oxidase-loaded liposomes for *in situ* amplified signal of electrochemical immunoassay on a handheld pH meter. New J Chem 43: 1372–1379
14. Wang J, Song M, Hu C, Wu K (2018) Portable, self-powered, and light-addressable photoelectrochemical sensing platforms using pH meter readouts for high-throughput screening of thrombin inhibitor drugs. Anal Chem 90:9366–9373
15. Jakhar S, Pundir C (2018) Preparation, characterization and application of urease nanoparticles for construction of an improved potentiometric pH urea biosensor. Biosens Bioelectron 100:242–250
16. Zhang C, Tang J, Huang L, Li Y, Tang D (2017) In-situ amplified voltammetric immunoassay for ochratoxin A by coupling a platinum nanocatalyst based enhancement to a redox cycling process promoted by an enzyme mimic. Microchim Acta 184:2445–2453
17. Abolhasan R, Mehdizadeh A, Rashidi M, Aghebati-Maleki L, Yousenfi M (2019) Application of hairpin DNA-based biosensor with various signal amplification strategies in clinical diagnosis. Biosens Bioelectron 129:164–174
18. Rayner P, Duckett S (2018) Signal amplification by reversible exchange (SABRE): from discovery to diagnosis. Angew Chem Int Ed 57:6742–6753
19. Ali M, Li F, Zhang Z, Zhang K, Kang D, Ankrum J, Le X, Zhao W (2014) Rolling circle amplification: a versatile tool for chemical biology, materials science and medicine. Chem Soc Rev 43:3324–2241
20. Warford A, Akar H, Riberio D (2014) Antigen retrieval, blocking, detection and visualization systems in immunohistochemistry: a review and practical evaluation of tyramide and rolling circle amplification systems. Methods 70:28–33
21. Mohsen M, Kool E (2016) The discovery of rolling circle amplification and rolling circle transcription. Acc Chem Res 49:2540–2550
22. Zhang K, Lv S, Lin Z, Li M, Tang D (2018) Bio-bar-code-based photoelectrochemical immunoassay for sensitive detection of prostate-specific antigen using rolling circle amplification and enzymatic biocatalytic precipitation. Biosens Bioelectron 101: 159–166
23. Zhang B, Liu B, Zhou J, Tang J, Tang D (2013) Additional molecular biological amplification strategy for enhanced sensitivity of monitoring low-abundance protein with dual nanotags. ACS Appl Mater Interfaces 5:4479–4485
24. Xiang Y, Lu Y (2011) Using personal glucose meters and functional DNA sensors to quantify a variety of analytical targets. Nat Chem 3: 697–703
25. Zhang B, Liu B, Tang D, Niessner R, Chen G, Knopp D (2012) DNA-based hybridization chain reaction for amplified bioelectronics signal and ultrasensitive detection of proteins. Anal Chem 84: 5392–5399
26. Aamna A, Talpur F, Kumar A, Tariq M, Muhammad A (2019) Synthesis of ultrasonic-assisted lead ion imprinted polymer as a selective sorbent for the removal of Pb^{2+} in a real water sample. Microchem J 146:1160–1168
27. Wang Y, Liu Z, Luo F, Peng H, Zhang S, Xie R, Ju X, Wang W, Faraj Y, Chu L (2019) A novel smart membrane with ion-recognizable nanogels as gates on interconnected pores for simple and rapid detection of trance lead(II) ions in water. J Membr Sci 575:28–37
28. Lu Z, Lin X, Zhang J, Dai W, Liu B, Mo G, Ye J, Ye J (2019) Ionic liquid/ploy-L-cysteine composite deposited on flexible and hierarchical porous laser-engraved graphene electrode for high-performance electrochemical analysis of lead ion. Electrochim Acta 295:514–523

29. Ding J, Liu Y, Zhang D, Yu M, Zhang X, Zhang D, Zhou P (2018) An electrochemical aptasensor based on gold@polypyrrole composite for detection of lead ions. Microchim Acta 185:545
30. Xiao S, Chen L, Xiong X, Zhang Q, Feng J, Deng S, Zhou L (2018) A new impedimetric sensor based on anionic intercalator for detection of lead ions with low cost and high sensitivity. J Electroanal Chem 827:175–180
31. Thirumalai M, Kumar S, Prabhakaran D, Sivaraman N, Maheswari M (2018) Dynamically modified C_{18} silica monolithic column for the rapid determination of lead, cadmium and mercury ions by reversed-phase high-performance liquid chromatography. J Chromatogr 1569:62–69
32. Wang H, Ma L, Fang B, Zhao Y, Hu X (2018) Graphene oxide-assisted Au nanoparticle strip biosensor based on GR-5 DNAzyme for rapid lead ion detection. Colloids Surf B 169:305–312
33. Li P, Li J, Bian M, Huo D, Hou C, Yang P, Zhang S, Shen C, Yang M (2018) A redox route for the fluorescence detection of lead ions in sorghum, river water and tap water and a desk study of a paper-based probe. Anal Methods 10:3256–3262